Received: 9 May 2022 | Accepted: 14 September 2022

DOI: 10.1111/iej.13836

ORIGINAL ARTICLE

INTERNATIONAL ENDODONTIC JOURNAL | WILEY

Isthmus morphology influences debridement efficacy of activated irrigation: A laboratory study involving biofilm mimicking hydrogel removal and high-speed imaging

Lieven Robberecht[1,2] | **Jérôme Delattre**[3] | **Maarten Meire**[1]

[1]Section of Endodontology, Department of Oral Health Sciences, Ghent University, Ghent, Belgium

[2]Department of Restorative Dentistry and Endodontics, Faculty of Odontology, Univ. Lille, Inserm, CHU Lille, U1008, Lille, France

[3]MABLAB 4490, Université de Lille, Lille, France

Correspondence
Lieven Robberecht, Faculty of Dentistry, Université de Lille, Place de Verdun, 59000 Lille, France.
Email: lieven.robberecht@univ-lille.fr

Funding information
Programme Investissement d'Avenir (French Government), Grant/Award Number: ULNE/ANR-16-IDEX-0004

Abstract

Aim: Little is known about the influence of isthmus morphology on the debridement efficacy of activated irrigation. The aim of this study was to investigate the influence of isthmus morphology on the debridement efficacy of laser-activated irrigation (LAI), EDDY and needle irrigation (NI), and to explain the methods of isthmus cleaning by LAI and EDDY.

Methodology: Four root canal models (apical diameter: 0.30 mm, taper: 0.06, curvature: 23°, length: 20 mm) were produced by CAD-CAM with different isthmus morphologies: long-wide (4 mm; 0.4 mm), long-narrow (4 mm; 0.15 mm), short-wide (2 mm; 0.4 mm) and short-narrow (2 mm; 0.15 mm). The isthmuses were filled with a hydrogel containing dentine debris. The canals were filled with irrigant and models were assigned to the following irrigation protocols ($n = 240$): needle irrigation (NI) with a 30G needle, Eddy, and LAI (2940 nm Er:YAG-laser, 15 Hz, 40 mJ, SWEEPS, tip at the canal entrance). Standardized images of the isthmuses were taken before and after irrigation, and the amount of removed hydrogel was determined using image analysis software and compared across groups using Kruskal–Wallis test followed by Dunn's multiple comparison. Visualization of the isthmus during activation was achieved using a high-speed camera. The pattern and speed of the flow in the isthmus as well as transient and stable cavitation were analysed using imaging software.

Results: Laser-activated irrigation, EDDY and NI removed more hydrogel in short-wide isthmuses than in narrow isthmuses ($p < .001$). LAI and EDDY removed more hydrogel than NI in every isthmus configuration ($p < .001$). EDDY showed eddies and stable cavitation, and LAI showed transient cavitation at each pulse, and pulsed horizontal flow with the highest particle speed in closed short isthmuses.

Conclusions: Isthmus morphology influences debridement in all irrigation groups. Short-wide isthmuses were the easiest to clean while narrow isthmuses were the most challenging to clean. Width seems to be a more critical anatomical parameter than length. LAI and EDDY resulted in the greatest biofilm removal and performed better than NI. EDDY produced eddies and stable cavitation in the isthmus, and LAI showed transient cavitation and pulsed horizontal flow.

KEYWORDS

Eddy, erbium laser, isthmus, root canal irrigation, sonic activation

INTRODUCTION

Irrigation is an essential aspect of chemomechanical root canal preparation. The irrigating solutions serve to clean the parts of the canal system that have escaped the mechanical instrumentation (Peters et al., 2001), to remove the smear layer (Mader et al., 1984) and accumulated hard tissue debris produced by these instruments (Paqué et al., 2011), along with removal of bacteria, toxins, and organic debris from the root canal in order to prevent or heal periapical disease.

The root canal anatomy of the mesial root of mandibular molar teeth can be extremely challenging, in part due to the high prevalence of isthmuses in these roots (Keles & Keskin, 2018; Tahmasbi et al., 2017). Isthmuses are narrow corridors or transverse anastomoses connecting two root canals (Weller et al., 1995). The presence of isthmuses was found to be as high as 85% for both mandibular first and second molars (Fan et al., 2008, 2009, 2010; Von Arx, 2005) and these isthmuses are found most frequently in the 3–6 mm section from the apex (de Pablo et al., 2010; Gu, Kim, et al., 2009; Gu, Wei, et al., 2009; Mannocci et al., 2005). Isthmus dimensions may vary. Their median (Q1, Q3) major and minor diameters are ranging from 2.725 (2.181, 3.204) mm to 0.070 (0.050, 0.113) mm, respectively (Yin et al., 2021). Isthmuses represent a considerable challenge for root canal shaping, cleaning and obturation. Their ribbon-shape with confined dimensions and their lateral extension from the main canal make them inaccessible to mechanical preparation (Leoni et al., 2017). This results in frequent clogging with dentinal debris (Paqué et al., 2009) whose removal with conventional irrigation methods is challenging (Leoni et al., 2017; Neelakantan et al., 2016). The residual micro-organisms and debris contained in the isthmus might lead to failure of orthograde treatment (Alves et al., 2016), failure of endodontic microsurgery (Kim et al., 2016) and leaking of the root filling (De–Deus et al., 2008).

The conventional root canal irrigation method is by means of a syringe with a needle. However, the penetration of the irrigant in the apical third and beyond the main canal is limited (Versiani et al. 2015), resulting in suboptimal cleaning of needle irrigation (NI). Irrigation efficacy can be optimized using irrigant activation techniques. These facilitate irrigant flow and distribution within the complex three-dimensional anatomy of the root canal system (Gu, Kim, et al., 2009; Gu, Wei, et al., 2009).

Eddy (EDDY) is a sonically activated irrigation device (Eddy; VDW). It operates a smooth polymer tip that oscillates at 6000 Hz by means of a sonic scaler. The manufacturer declares that the cleaning is enhanced by cavitation and acoustic streaming within the irrigant, but it was reported that no cavitation occurs with sonically oscillating instruments as the movement of the tip is below the threshold of cavitation (Macedo et al., 2014; Swimberghe et al., 2019).

Laser-activated irrigation (LAI) is another activation method, shown very efficient in removing debris (Arslan et al., 2014; De Moor et al., 2010; Swimberghe et al., 2019). Pulsed erbium lasers produce optical cavitation, causing expansion and implosion of a vapour bubble at the fibre tip (Song et al., 2004), responsible for very rapid fluid movement, secondary cavitation bubbles and photoacoustic effects (Blanken et al., 2009; Gregorcic et al., 2012). Recently, this phenomenon can be amplified by generating a second pulse extremely fast after the first one, thereby accelerating the collapse of the first bubble and increasing photoacoustic effects (SWEEPS; Fotona) (Lukač & Jezeršek, 2018).

Previous studies have addressed the cleaning of isthmuses by various irrigant activation devices (Iandolo et al., 2021; Rödig et al., 2019; Rodrigues et al., 2021; Swimberghe et al., 2019). The majority of these studies investigated the removal of hard tissue debris from the isthmus in mesial roots of extracted mandibular molars using micro-CT. A recent systematic review with network-meta-analysis addressing hard tissue debris reduction from the mesial roots of mandibular molars, found that none of the activation methods rendered the canal anatomy completely free of hard tissue debris, but laser-activated irrigation groups fared better than activation protocols based on intracanal placement of oscillating tips or needles (Natansabapathy et al., 2021). Swimberghe et al. (2019), investigating the removal of a biofilm-mimicking hydrogel containing dentin debris from the isthmus in an acrylic isthmus model, came to similar conclusions. Malentacca et al. (2018) investigated the efficacy of different activated irrigation techniques in removal of pulp tissue from the isthmus in a transparent extracted tooth. They found ultrasonically driven techniques to be superior than negative apical pressure. Alsubait et al. (2021) investigated the isthmus cleanliness in horizontal sections of the roots of mandibular molars after different adjunctive irrigation steps. They found that passive ultrasonic irrigation, mechanical activation with the XP-endo Finisher and manual dynamic irrigation with gutta-percha equally improved canal cleanliness.

Although such experiments provide valuable data, they only allow a partial understanding of the involved mechanisms during activation of the irrigant, as human teeth lack standardization and studies using artificial isthmus models use single and simplified anatomies and do not consider the large variability in isthmus morphology found clinically. In order to better understand the influence of various morphological isthmus parameters on the

irrigation, it is necessary to provide a standardized model with biomimetic morphology.

Therefore, the aim of this study was to investigate the influence of isthmus morphology (length and width) on the removal of an artificial biofilm by LAI compared with EDDY and NI as control in new realistic 3D-printed isthmus models; and to explain the methods of action of LAI and EDDY by means of high-speed imaging in these models. The null hypothesis was that there is no influence of isthmus morphology on the removal of artificial biofilm during activated irrigation.

MATERIALS AND METHODS

The manuscript of this laboratory study has been written according to Preferred Reporting Items for Laboratory studies in Endodontology (PRILE) 2021 guidelines (Figure S1).

3D-printed isthmus models

A micro-CT STL dataset of an intact mandibular first molar with a resolution of 20 µm served as the basis for development of the model. After loading the data in CAD software (Catia; Dassault systèmes), only the two mesial root canals were kept and used as a pattern/template to design a fully editable 3D virtual model of the root canal system. The mesial canals were modified in order to obtain an apical canal size of 0.30 mm, a 0.06 taper, a 23° curvature (Schneider, 1971). A ribbon-shaped isthmus was designed, connecting the two canals and providing a Vertucci type VI configuration to the root canal system. The floor and the roof of the isthmus were positioned at 3 and 6 mm from the apical foramina, respectively. The entire isthmus was given a convex shape both in buccolingual and mesiodistal direction, conform isthmus morphology observed *in vivo* (Keles & Keskin, 2018). An access cavity (width: 3 or 7 mm, length: 9 mm, height: 5 mm) was designed, mimicking the anatomical reality. The canals were 15 mm long (Figure 1). Four different root canal systems were designed according to the length (L, bucco-lingual distance) and width (W, mesiodistal distance) of the isthmus: long-wide (L: 4 mm; W: 0.4 mm), short-wide (L: 2 mm; W: 0.4), long-narrow (L: 4 mm; W: 0.15) and short-narrow (L: 2 mm; W: 0.15) (Figure 2). The 3D models were created in a virtual block. A removable part was designed at the level of the isthmus to allow access to the isthmus. Screw holes were accommodated to allow firm attachment of the removable part. Data were transferred to stereolithographic software (Preform; FormLabs) and equipment (3D Form 2, FormLabs) in. STL format for 3D-printing (resolution: 25 µm, resin: Clear V4). The 3D-printed models were washed in isopropyl alcohol for 20 min to remove noncured resin (Form Wash, FormLabs). Finally, the models were postcured at 60°C for 30 min (Form Cure, FormLabs) and the supporting pillars were removed.

Artificial biofilm

The artificial biofilm was a hydrogel based on the work of Macedo et al. (2014) and modified by Swimberghe et al. (2019) by incorporating dentine debris. Three grams of gelatin (Merck) and 0.03 g hyaluronan (sodium hyaluronate 95%; Fisher) were dissolved in 22.5 ml deionized water

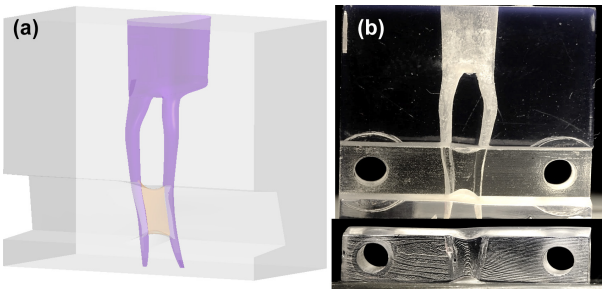

FIGURE 1 Virtual and 3D-printed root canal model. A removable part facilitates the placement of the artificial biofilm in the isthmus.

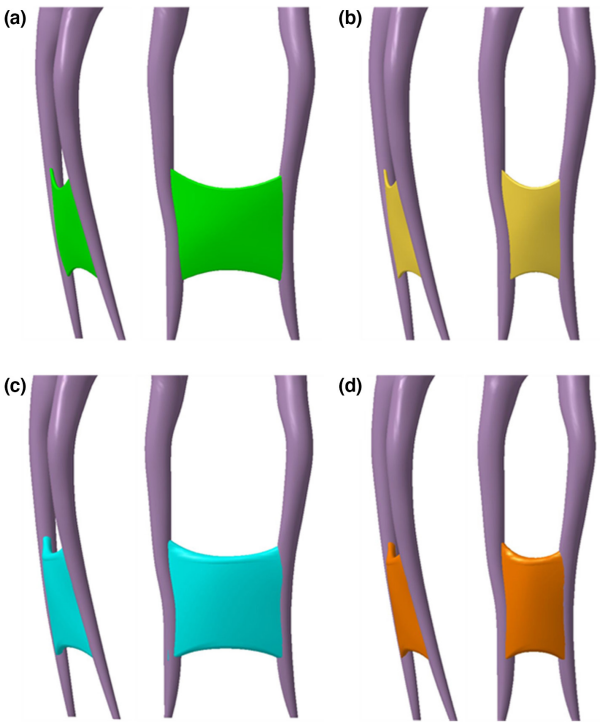

FIGURE 2 Virtual root canal anatomy (lateral and mesial views) of 3D-printed root canal models: Long-narrow (a) short-narrow (b) long-wide (c) and short-wide (d) isthmus morphologies.

at 40°C under stirring. 0.1 g hollow glass spheres (diameter: 10 μm; density: 1100 kg·m^{-3}; Sigma Aldrich) and a red dye were added to the mixture. Dentin debris was obtained by grinding bovine dentine and sieving the powder with a mesh 100 sieve to obtain particles smaller than 150 μm. Debris was added to the hydrogel (30/70 w/w) to simulate hard tissue debris accumulation in the isthmus that occurs during the mechanical preparation. The artificial biofilm was gently positioned in the isthmus under operating microscope. The volume of artificial biofilm was standardized and corresponded to the volume of the isthmuses. The 3D-printed models were closed and tightened with two screws and two nuts, the apical foramina were sealed with wax to obtain a closed system and were filled with water.

Experimental groups

After assembly, the models were randomly assigned to one of three irrigant activation groups. This was done for the four isthmus designs, and each irrigation condition was repeated 20 times, conform the sample size calculation in Choi et al., 2021, yielding a total of 240 tests. The irrigant used was water.

In the NI group (control), canals were irrigated by means of a 3-ml manual syringe equipped with a 30G notched needle (Vista Appli-vac 30G; Vista Dental Products). A gentle up-and-down movement was applied to the needle ranging from 1- to 5 mm from the apex with a flow rate of 3 ml/20 s. Each root canal was irrigated for 3 × 20 s.

In the EDDY group, activation occurred with the Eddy device (VDW, GmbH). The Eddy tip was driven by a sonic scaler (Proxeo, W&H) following manufacturer's instructions (6 kHz) and was moved up and down over a distance of 4 mm, starting 1 mm from the apical terminus. Irrigant was continuously replenished. Activation was also performed for 2 × 30 s and the canals were flushed with 3 ml (3 ml/20 s) water in-between and after each activation cycle.

In the LAI samples, an Er:YAG-laser (LightWalker; Fotona), equipped with a H14 handpiece (Fotona) and a flat fibre tip (SWEEPS 400/9) was used to activate the irrigant in auto-SWEEPS mode (40 mJ, 15 Hz, 0.6 w, air and water turned off). The fibre tip was positioned 2 mm above each root canal entrance, and activation was performed 2 × 30 s with irrigant being continuously replenished during activation. The canals were flushed with 3 ml (3 ml/20 s) irrigant in between and after each activation cycle using a 30G notched needle (Vista Appli-vac 30G).

Irrigation and activation were performed in both mesiobuccal and mesiolingual canals. During irrigation, the operator was blinded to the isthmuses by means of a silicone cover, covering the outer walls of the models.

Determination of hydrogel removal

Standardized high resolution (3216 × 2136 pixels) images of the model were taken before and after irrigant activation using a custom-made setup, allowing the exact repositioning of each 3D-printed isthmus model (Nikon D300 with a 120-mm macro lens (Medical Nikkor [1/1], f = 4)). The hydrogel-covered isthmus area was determined in each image using image analysis software (Fiji, https://imagej.net/Fiji). To this end, the isthmus was outlined and a segmentation procedure (Simple Interactive Object Extraction in Fiji) was then carried out in this area to select the hydrogel. The percentage of remaining hydrogel was calculated as the number of selected pixels after activation relative to the number of pixels before activation, and the percentage of biofilm removal was deduced from this. Values were stored in a database (IBM SPSS Statistics version 27; SPSS Inc.).

High-speed imaging and analysis

High-speed imaging was used to analyse irrigant flow in the isthmus and to detect the presence of transient or stable cavitation by each activation method. This was done for both open and closed isthmus models. In order to produce a closed isthmus, one of the canals was blocked by means of silicon The isthmus models were positioned in front of a Fastcam SA-X2 camera (Photron) equipped with a micro lens zoom system. A high intensity LED light source (LA-HDF7010; Hayashi) illuminated the model from behind. Recordings were done both in empty isthmus models and models with the isthmus closed at one side. In order to visualize irrigant flow, glass microspheres (0.1 g; 10 μm diameter, density: 1100 kg/m^3; Sigma Aldrich) were added to the irrigant, and irrigant activation cycles were recorded at a frame rate of 5000 fps. In order to study the transient and stable cavitation, activation cycles were recorded at a frame rate of 30 000 fps, no glass particles added. In this way, high-speed videos were obtained for the two activation methods in the four isthmus morphologies. Photron Fastcam Viewer V4 software (Photron) was used to measure the maximum speed of the particles (three measurements per video) and to describe the flow pattern in the isthmus, and to describe cavitation phenomena in the isthmus.

Statistical analysis

Hydrogel removal data were analysed using SPSS Statistics software (IBM) ($\alpha = 5\%$). As the data were not normally distributed (according to Kolmogorov–Smirnov test), the Kruskal–Wallis test followed by Dunn's multiple comparison *post hoc* test and Bonferroni correction was performed

to test for differences between isthmus configurations, and between activation methods.

RESULTS

Hydrogel removal

Hydrogel removal by the three irrigation protocols in the four isthmus types is summarized in Table 1 and graphically presented in Figure 3. LAI, EDDY and NI showed significantly greater biofilm removal in short-wide isthmuses than in narrow isthmuses ($p < .001$). No significant difference in biofilm removal was found between long and short isthmuses of the same width, regardless of irrigation protocol ($p > .05$), except for LAI who showed greater biofilm removal in short-wide than in long-wide isthmuses ($p < .001$). LAI and EDDY resulted in significantly greater biofilm removal than NI in every isthmus configuration ($p < .001$), but no significant difference was found between LAI and EDDY ($p > .05$). Representative postoperative images of each isthmus type are shown in Figure 4.

High-speed imaging

EDDY produced a continuous and steady flow, while the flows produced by LAI were pulsed: short and fast flows were followed by periods of relative little flow (Videos S1 and S2). Irrigant flow patterns in the isthmus are shown in Figure 5.

In open isthmuses, the general pattern with both activation devices was fluid displacement from the activated to the other root canal. Activation by EDDY produced revolving currents (eddies) in the isthmus; their location and number differed with the isthmus type (Figure 4). Maximum fluid speeds ranged between 0.3 ± 0.0 m/s (in the long narrow type) and 2.1 ± 0.4 m/s (in the short wide type). Fluid speeds by LAI ranged between 0.5 ± 0.1 m/s (in the long wide type) and 3.8 ± 0.9 m/s (in the short narrow type). The short-wide isthmuses displayed eddies for both activation methods and showed the most marked ones (Figure 5) (video provided in Videos S3–S18).

In closed isthmuses, fluid displacement from one canal to the other did not take place. EDDY, as in the open isthmuses, produced steady revolving currents, fluid speeds now ranging between 0.1 ± 0.0 m/s and 0.6 ± 0.1 m/s. LAI showed very rapid horizontal back-and-forth movements of the irrigant with every pulse (fluid speeds from 0.5 ± 0.1 m/s to 3.9 ± 0.1 m/s). LAI had higher fluid speed in closed short isthmuses than in long isthmuses and in EDDY.

The high-speed recordings at 30 000 fps revealed the events taking place in the canals and the isthmus during LAI and EDDY activation. These demonstrated stable cavitation of pre-existing bubbles in each isthmus with EDDY, oscillating at 5988 Hz (Video S2).

With LAI, there was very limited liquid movement in the canal system during the period in between 2 pulses (pulse pairs in fact). When the laser pulse produced a primary cavitation bubble above the canal entrance, appearance/growth of bubbles of order of magnitude of 0.5 mm over the entire length of both canals, and 0.25 mm in the isthmus was seen. These bubbles appeared rapidly and imploded soon after implosion of the primary bubble. This caused a vertical liquid movement in the canals, and a horizontal movement in the isthmus. The second pulse of the pair, arriving at a variable delay time after the first pulse, evoked the same events, hence causing a second sequence of very rapid irrigant movement (video provided in Video S1).

DISCUSSION

The present data demonstrate that the three irrigation methods showed a better cleaning of short-wide isthmuses than narrow isthmuses. No differences in hydrogel removal were found between long and short isthmuses of the same width except for LAI in the wide isthmuses. The null hypothesis, stating that there is no influence of isthmus morphology on the removal of artificial biofilm,

TABLE 1 Removed artificial biofilm (%) (median [Q1; Q3]) by needle activation (NI), Eddy (EDDY) and laser activated irrigation (LAI) in different isthmus morphologies ($n = 20$/group)

Isthmus morphology	NI	EDDY	LAI
Long-narrow	0.8 (0.3; 2.9)^{abΩ}	15.9 (8.7; 36.7)^{aπ}	16.7 (12.3; 39.6)^{bρ}
Short-narrow	0.4 (0.2; 1.5)^{cdα}	27.7 (10.6; 45.2)^{cβ}	40.4 (33.8; 61.7)^{dσ}
Long-wide	4.1 (1.5; 22.4)^{ef}	39.8 (20.2; 48.8)^{e}	50.6 (34.3; 55.1)^{fP}
Short-wide	31.7 (23.1; 38.6)^{ghαΩ}	88.6 (53.6; 100,0)^{gπβ}	100.0 (80.5; 100.0)^{hρσP}

Note: Similar Arabic superscript letters indicate a significant difference between the irrigation groups (in the row) ($p < .001$). Similar Greek symbols indicate a significant difference between the isthmus morphologies (in the column) ($p < .001$).

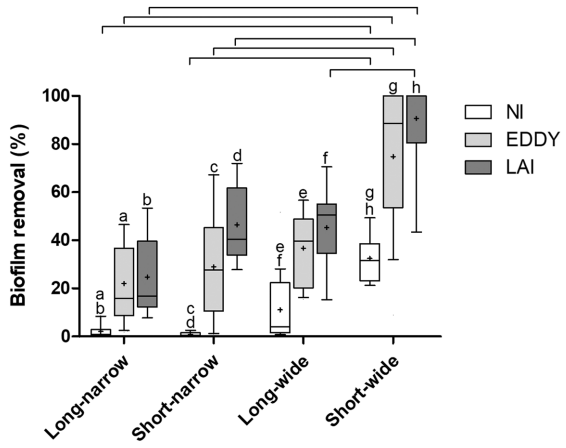

FIGURE 3 Boxplots of biofilm removal after irrigation by needle activation (NI), EDDY (EDDY) and laser activated irrigation (LAI) in different isthmus morphologies. Bars indicate significant differences between isthmus types (per irrigation method). The same letter indicates significant differences between the irrigation methods (per isthmus type) ($p < .05$).

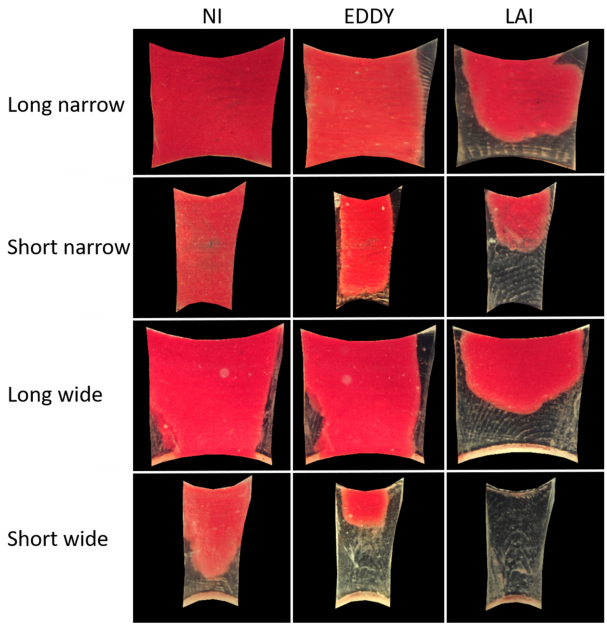

FIGURE 4 Hydrogel patterns after activation per group in different isthmus morphologies

has to be rejected. High-speed imaging disclosed steady irrigant eddies in the isthmus during EDDY activation and pulsed horizontal oscillation during LAI.

This study is the first to investigate the impact of isthmus anatomy on the efficacy of irrigant activation. In addition, newly developed 3D-printed models were used, displaying a very realistic 3D root canal anatomy, reproducing complex shapes and irregularities found in human teeth. The use of these models helps to overcome the problems due to high morphological variability of natural teeth (Caron et al., 2010) and provides a very high degree of standardization by fabricating strictly identical root canal systems with different isthmus shapes but with otherwise identical dimensions (Macedo et al., 2014). While similar isthmus models have been used in previous studies (De Meyer et al., 2017; Meire et al., 2016; Swimberghe et al., 2019; Swimberghe, Buyse, et al., 2021) providing valuable information on the cleaning efficiency of different irrigant-activation devices in straight-, curved canals and isthmuses, the design of these models is basic, lacking any canal or isthmus curvature. In this respect, the current model takes the root canal and isthmus morphology much closer to the anatomical reality. The removable part facilitates direct application of the hydrogel in the isthmus, and the transparency of the models enables accurate determination of hydrogel removal (Swimberghe, Buyse, et al., 2021). The position of the isthmuses was standardized at 3 mm from the apical foramina (Gu, Kim, et al., 2009; Gu, Wei, et al., 2009; Villas-Boas et al., 2011), and their dimensions were determined to correspond to the average maximum and minimum length and width values found in the literature (Keles & Keskin, 2018). The curvature of the root canals was set at 23° to match with generally reported curvatures in mandibular molars as well (Gu et al., 2010). The isthmus in this study was irrigated from both sides to simulate clinical reality.

The biofilm-mimicking hydrogel used to fill the isthmuses has been used in previous studies (Swimberghe et al., 2019; Swimberghe, Buyse, et al., 2021) and is based on the hydrogel described by Macedo et al. (2014), known as a highly standardized and controllable natural biofilm substitute. Bovine dentine debris was added, in order to approach the clinical situation where hard tissue debris generated by mechanical preparation is forced into the isthmus (Paqué et al., 2009). The present experimental setup entailed an extreme standardization, allowing the most subtle and differentiating comparison between the various test conditions. In addition to anatomical standardization of the models, the hydrogels were prepared under the same thermal conditions in order to control their viscoelastic behaviour and guarantee their stability (Macedo et al., 2014). Hydrogel placement was standardized as well. The irrigant-activation protocols were standardized with regard to timing, tip positioning, flow rates, adherence to the manufacturer's instructions and blinding of the operator. The acquisition of the images was also standardized in terms of sample positioning, light and background. The image analysis was the same for each group by using the same saved ROIs and segmentators in FIJI to select the hydrogel. This minimized operator bias during the image analysis procedure.

Overall, short-wide isthmus types were best cleaned, regardless of the irrigation method. This result is not illogical, as wide isthmuses offer more hydrogel contact surface and more space for irrigant flow compared with

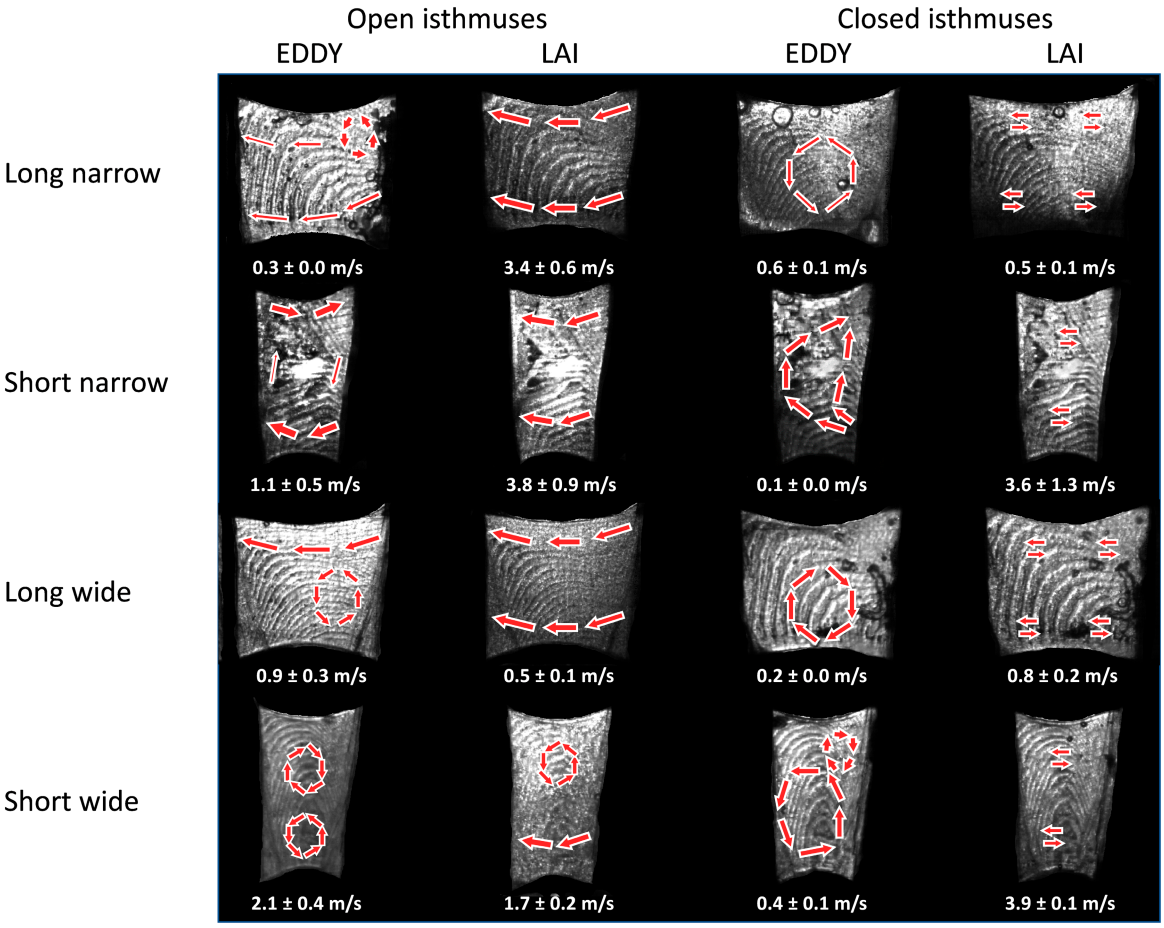

FIGURE 5 Flow patterns and maximum particle speed after activation per group in different isthmus morphologies captured by shadowgraphy. Activation was performed in the right root canal.

small isthmuses, and the short intercanal distance poses less challenges than the long one. NI had very little effect on the hydrogel in the narrow isthmus types. The absence of significant differences in cleaning between long and short isthmuses with a fixed width suggests that the width of the isthmus is more critical than its length.

EDDY and LAI cleaned the isthmuses markedly better than NI. This corroborates earlier findings by De Moor et al., 2010, Conde et al., 2017, Haupt et al., 2020, Güven et al., 2021 and Swimberghe, Buyse, et al., 2021, and supports the use of an adjunctive irrigant activation step after canal preparation. While the mean/median hydrogel removal by LAI was higher than that by EDDY in every condition, this difference was not significant. When applying LAI, the fibre tip is positioned above the root canal entrance. This is in contrast with EDDY, requiring intracanal tip positioning to exert any effect in the isthmus. LAI has been shown very efficient in removing debris in straight canals (de Groot et al., 2009; De Moor et al., 2010), isthmuses (Swimberghe et al., 2019) and curved canals (Swimberghe, Buyse, et al., 2021). The irrigant dynamics and flow generated during LAI seem not affected by the root canal curvature (Peeters et al., 2015). In contrast, introduction of an EDDY tip in a curved canal results in tip deflexion and wall contact, generating tensions that reduce its movement and oscillation, leading to a weaker streaming of the irrigant (Swimberghe, Buyse, et al., 2021). The absence of significant differences between EDDY and LAI may also be due to high Q1-Q3 ranges in both groups.

To date, no data are available regarding the physical mechanisms involved during LAI and EDDY activation in isthmuses. Therefore, high-speed imaging was used to elaborate on this. A typical shadowgraphy setup was followed that is relevant to visualize bubbles and solid particles that have a different refractive index than water (Gregorcic et al., 2012). This permits visualization of cavitation, but gives no information about the streaming of the irrigant. Therefore, glass particles were added in a second run of high-speed imaging to disclose the fluid movements within the isthmus. In open isthmuses, EDDY and LAI provoked irrigant displacement from the activated canal towards the empty root canal. Closed isthmuses were also investigated to mimic the clinical situation of an isthmus clogged with organic and inorganic debris at

the start of activation. No such streaming was observed in closed isthmuses.

The recordings disclosed steady circular irrigant eddies in the isthmus during EDDY activation. This was the case in every isthmus morphology. In this respect, EDDY does credit to its name. Fluid speeds generated by EDDY were higher in wide isthmuses compared with narrow isthmuses. The fluid pattern observed with LAI was markedly different: LAI generated 2 distinct and repetitive flow patterns: pulsed horizontal flow in open isthmuses, and horizontal back-and-forth flow in closed isthmuses (see additional material). Su et al. (2020), using particle image velocimetry, demonstrated that LAI activates a so-called "breath mode" during irrigation, represented by a back-and-forth vertical liquid movement along the main root canal in a closed system. In the situation of a closed isthmus, these movements become horizontal as the isthmus becomes a lateral extension of the main canal. This "breath mode" was not observed in open isthmuses. Instead, a circular flow (from the activated canal, through the isthmus, in the nonactivated canal, over the pulp chamber, back in the activated canal) was observed. This is likely explained by the fact that the first (apically directed) fluid movement of the breath mode does not encounter any opposing pressure and is evacuated through the isthmus in the connected canal.

In closed isthmuses, LAI had higher maximum particle speed than EDDY, and the speed was the highest in the short isthmuses. This is in line with the biofilm removal patterns observed in this work, showing that short isthmuses were also the best cleaned by LAI. The mean values measured remain in the range of those measured in previous works at 0.43 m/s and 1.3 m/s in main root canals (Koch et al., 2016). Interestingly, with EDDY, fluid speeds seemed higher in wide isthmuses compared with small isthmuses, while with LAI, the opposite pattern was observed. When matching the fluid speed with the biofilm removal, higher speeds resulted in higher hydrogel removal for EDDY, but not in the case of LAI. Other factors than fluid speed might thus be involved in debridement and should be further investigated. For example, acoustic effect, typically generated by LAI may account for this. The present methodology however is unable to disclose these.

The present methodology also has its drawbacks. Despite its recognition as a biofilm substitute for research purposes, the hydrogel offers a simplified representation of the natural biofilm and it has a weaker adhesion to the synthetic model's walls than a natural biofilm in a tooth (Boutsioukis et al., 2022). In this respect, the use of a mature multispecies endodontic biofilm is more realistic, but also comes with challenges to adequately quantify biofilm removal (Swimberghe, Crabbé, et al., 2021). Another potential limitation of this work is the necessity to use water instead of NaOCl as irrigant because the NaOCl decolorizes and provokes a surface dissolution of the hydrogel. In this respect, the present results represent mainly the physical action/effect of the various activated irrigation regimen, not any chemical effect. There are other potential consequences of the use of water instead of NaOCl as the irrigant. de Groot et al. (2009) observed larger bubbles and more intense cavitation when laser-activating NaOCl compared with water. Similarly, Cai et al. (2022) demonstrated stronger cavitation effects and fluid dynamics with 1% or 2.5% NaOCl than with saline during PIPS activation. This suggests that the debriding action of LAI potentially is higher with the use of NaOCl. When using activation systems based on oscillating tips, the use of NaOCl can also affect the debriding action due to the formation of small gas bubbles. These bubbles may hinder debridement, as described for ultrasonically activated irrigation by Macedo et al. (2014). Whether this also affects EDDY activation, remains unclear. In addition, fluid speed measurements were not as accurate as those obtained by more advanced techniques such as particle image velocimetry (Su et al., 2020).

CONCLUSION

Within the limitations of this laboratory study, it is possible to conclude that the isthmus morphology influences debridement efficacy of activated irrigation. Short-wide isthmuses were the easiest to clean, while narrow isthmuses were the most challenging to clean. Isthmus width seems to be a more critical anatomical parameter than isthmus length. LAI and EDDY resulted in the greater hydrogel removal than NI. EDDY produced eddies and stable cavitation in the isthmus, and LAI showed transient cavitation and pulsed horizontal flow.

AUTHOR CONTRIBUTIONS

Conception: LR, MM; Design: LR, JD, LR; Fundings: LR; Materials: LR, JD, MM; Data collection: LR; Analysis: LR, MM; Literature review: LR, MM; Writers: LR, JD, MM.

FUNDING INFORMATION

This study was supported by the French government through the Programme Investissement d'Avenir (I-SITE ULNE/ANR-16-IDEX-0004 ULNE) managed by the Agence Nationale de la Recherche.

CONFLICT OF INTEREST

The authors declare no conflict of interest.

DATA AVAILABILITY STATEMENT

The data that support the findings of this study are available from the corresponding author upon reasonable request.

ORCID

Lieven Robberecht https://orcid.org/0000-0003-0538-3023
Maarten Meire https://orcid.org/0000-0001-6661-3772

REFERENCES

Alsubait, S., Alshaibani, Y., Alshehri, N., Alnuwaiser, N., Alajimi, T., Almaflehi, N. et al. (2021) Efficacy of different endodontic Irrigant activation techniques on debris removal from the mesial root canal system of mandibular molars. *The Journal of Contemporary Dental Practice*, 22, 231–236.

Alves, F.R., Andrade–Junior, C.V., Marceliano–Alves, M.F., Pérez, A.R., Rôças, I.N., Versiani, M.A. et al. (2016) Adjunctive steps for disinfection of the mandibular molar root canal system: a correlative bacteriologic, micro–computed tomography, and cryopulverization approach. *Journal of Endodontics*, 42, 1667–1672.

Arslan, H., Capar, I.D., Saygili, G., Gok, T. & Akcay, M. (2014) Effect of photon-initiated photoacoustic streaming on removal of apically placed dentinal debris. *International Endodontic Journal*, 47, 1072–1077.

Blanken, J., De Moor, R.J., Meire, M. & Verdaasdonk, R. (2009) Laser induced explosive vapor and cavitation resulting in effective irrigation of the root canal. Part 1: a visualization study. *Lasers in Surgery and Medicine*, 41, 514–519.

Boutsioukis, C., Arias-Moliz, M.T. & Chavez de Paz, L.E. (2022) A critical analysis of research methods and experimental models to study irrigants and irrigation systems. *International Endodontic Journal*, 55, 295–329.

Cai, C., Wen, C., Guan, L. & Huang, Y. (2022) Influence of sodium hypochlorite concentration on cavitation effect and fluid dynamics induced by photon-induced photoacoustic streaming (PIPS): a visualization study. *Lasers in Medical Science*, 37, 2537–2544.

Caron, G., Nham, K., Bronnec, F. & Machtou, P. (2010) Effectiveness of different final irrigant activation protocols on smear layer removal in curved canals. *Journal of Endodontics*, 36, 1361–1366.

Choi, M.J., Kim, M.A., Choi, Y., Neelakantan, P., Yu, M.K. & Min, K.S. (2021) A three-dimensionally printed model to assess biofilm removal by ultrasonically activated irrigation. *International Endodontic Journal*, 54, 1871–1877.

Conde, A.J., Estevez, R., Lorono, G., Valencia de Pablo, O., Rossi-Fedele, G. & Cisneros, R. (2017) Effect of sonic and ultrasonic activation on organic tissue dissolution from simulated grooves in root canals using sodium hypochlorite and EDTA. *International Endodontic Journal*, 50, 976–982.

de Groot, S.D., Verhaagen, B., Versluis, M., Wu, M.K., Wesselink, P.R. & van der Sluis, L.W. (2009) Laser-activated irrigation within root canals: cleaning efficacy and flow visualization. *International Endodontic Journal*, 42, 1077–1083.

De Meyer, S., Meire, M.A., Coenye, T. & De Moor, R.J. (2017) Effect of laser-activated irrigation on biofilms in artificial root canals. *International Endodontic Journal*, 50, 472–479.

De Moor, R.J., Meire, M., Goharkhay, K., Moritz, A. & Vanobbergen, J. (2010) Efficacy of ultrasonic versus laser-activated irrigation to remove artificially placed dentin debris plugs. *Journal of Endodontics*, 36, 1580–1583.

de Pablo, O.V., Estevez, R., Peix Sanchez, M., Heilborn, C. & Cohenca, N. (2010) Root anatomy and canal configuration of the permanent mandibular first molar: a systematic review. *Journal of Endodontics*, 36, 1919–1931.

De–Deus, G., Reis, C., Beznos, D., Gruetzmacher de Abranches, A.M., Countinho-Filho, T. & Paciornik, S. (2008) Limited ability of three commonly used thermoplasticized gutta-percha techniques in filling oval-shaped canals. *Journal of Endodontics*, 34, 1401–1405.

Fan, B., Min, Y., Lu, G., Yang, J., Cheung, G.S. & Gutmann, J.L. (2009) Negotiation of C-shaped canal systems in mandibular second molars. *Journal of Endodontics*, 35, 1003–1008.

Fan, B., Pan, Y., Gao, Y., Fang, F., Wu, Q. & Gutmann, J.L. (2010) Three-dimensional morphologic analysis of isthmuses in the mesial roots of mandibular molars. *Journal of Endodontics*, 36, 1866–1869.

Fan, W., Fan, B., Gutmann, J.L. & Fan, M. (2008) Identification of a C-shaped canal system in mandibular second molars. Part III. Anatomic features revealed by digital subtraction radiography. *Journal of Endodontics*, 34, 1187–1190.

Gregorcic, P., Jezersek, M. & Mozina, J. (2012) Optodynamic energy-conversion efficiency during an Er:YAG-laser-pulse delivery into a liquid through different fiber-tip geometries. *Journal of Biomedical Optics*, 17, 075006.

Gu, L., Wei, X., Ling, J. & Huang, X. (2009) A microcomputed tomographic study of canal isthmuses in the mesial root of mandibular first molars in a Chinese population. *Journal of Endodontics*, 35, 353–356.

Gu, L.S., Kim, J.R., Ling, J., Choi, K.K., Pashley, D.H. & Tay, F.R. (2009) Review of contemporary irrigant agitation techniques and devices. *Journal of Endodontics*, 35, 791–804.

Gu, Y., Lu, Q., Wang, P. & Ni, L. (2010) Root canal morphology of permanent three-rooted mandibular first molars: part II—measurement of root canal curvatures. *Journal of Endodontics*, 36, 1341–1346.

Güven, Y., Uygun, A.D. & Arslan, H. (2021) Efficacy of EDDY, ultrasonic activation, XP-endo finisher and needle irrigation on the removal of mTAP from artificially created grooves in root canals. *Australian Endodontic Journal*, 47, 639–644.

Haupt, F., Meinel, M., Asanka Gunawardana, A. & Hülsmann, M. (2020) Effectiveness of different activated irrigation techniques on debris and smear layer removal from curved root canals: a SEM evaluation. *Australian Endodontic Journal*, 46, 40–46.

Iandolo, A., Amato, M., Abdellatif, D., Barbosa, A.F.A., Pantaleo, G., Blasi, A. et al. (2021) Effect of different final irrigation protocols on pulp tissue dissolution from an isthmus model. *Australian Endodontic Journal*, 47, 538–543.

Keles, A. & Keskin, C. (2018) A micro-computed tomographic study of band-shaped root canal isthmuses, having their floor in the apical third of mesial roots of mandibular first molars. *International Endodontic Journal*, 51, 240–246.

Kim, S., Jung, H., Kim, S., Shin, S.J. & Kim, E. (2016) The influence of an isthmus on the outcomes of surgically treated molars: a retrospective study. *Journal of Endodontics*, 42, 1029–1034.

Koch, J.D., Jaramillo, D.E., DiVito, E. & Peters, O.A. (2016) Irrigant flow during photon-induced photoacoustic streaming (PIPS) using particle image velocimetry (PIV). *Clinical Oral Investigations*, 20, 381–386.

Leoni, G.B., Versiani, M.A., Silva-Sousa, Y.T., Bruniera, J.F.B. & Sousa-Neto, M.D. (2017) Ex vivo evaluation of four final irrigation protocols on the removal of hard-tissue debris from the mesial root canal system of mandibular first molars. *International Endodontic Journal*, 50, 398–406.

Lukač, N. & Jezeršek, M. (2018) Amplification of pressure waves in laser-assisted endodontics with synchronized delivery of Er:YAG laser pulses. *Lasers in Medical Science*, 4, 823–833.

Macedo, R., Verhaagen, B., Rivas, D.F., Versluis, M., Wesselink, P. & van der Sluis, L. (2014) Cavitation measurement during sonic and ultrasonic activated irrigation. *Journal of Endodontics*, 40, 580–583.

Mader, C.L., Baumgartner, J.C. & Peters, D.D. (1984) Scanning electron microscopic investigation of the smeared layer on root canal walls. *Journal of Endodontics*, 10, 477–483.

Malentacca, A., Uccioli, U., Mannocci, F., Bhuva, B., Zangari, D., Pulella, C. et al. (2018) The comparative effectiveness and safety of three activated irrigation techniques in the isthmus area using a transparent tooth model. *International Endodontic Journal*, 51, e35–e41.

Mannocci, F., Peru, M., Sherriff, M., Cook, R. & Pitt Ford, T.R. (2005) The isthmuses of the mesial root of mandibular molars: a micro-computed tomographic study. *International Endodontic Journal*, 38, 558–563.

Meire, M.A., Havelaerts, S. & De Moor, R.J. (2016) Influence of lasing parameters on the cleaning efficacy of laser-activated irrigation with pulsed erbium lasers. *Lasers in Medical Science*, 31, 653–658.

Natansabapathy, V., Natanasabapathy, V., Arul, B., Srinivasan, V., Santosh, S.S., Vasudevan, A. et al. (2021) Removal of accumulated hard tissue debris from mesial root of mandibular molars evaluated using micro-CT – a systematic review and network meta-analysis. *Evidence-Based Dentistry*, 35, e123.

Neelakantan, P., Devaraj, S. & Jagannathan, N. (2016) Histologic assessment of debridement of the root canal isthmus of mandibular molars by irrigant activation techniques ex vivo. *Journal of Endodontics*, 42, 1268–1272.

Paqué, F., Boessler, C. & Zehnder, M. (2011) Accumulated hard tissue debris levels in mesial roots of mandibular molars after sequential irrigation steps. *International Endodontic Journal*, 44, 148–153.

Paqué, F., Laib, A., Gautschi, H. & Zehnder, M. (2009) Hard-tissue debris accumulation analysis by high-resolution computed tomography scans. *Journal of Endodontics*, 35, 1044–1047.

Peeters, H.H., De Moor, R.J. & Suharto, D. (2015) Visualization of removal of trapped air from the apical region in simulated root canals by laser-activated irrigation using an Er,Cr:YSGG laser. *Lasers in Medical Science*, 30, 1683–1688.

Peters, O.A., Schonenberger, K. & Laib, A. (2001) Effects of four Ni-Ti preparation techniques on root canal geometry assessed by micro computed tomography. *International Endodontic Journal*, 34, 221–230.

Rödig, T., Koberg, C., Baxter, S., Konietschke, F., Wiegand, A. & Rizk, M. (2019) Micro-CT evaluation of sonically and ultrasonically activated irrigation on the removal of hard-tissue debris from isthmus-containing mesial root canal systems of mandibular molars. *International Endodontic Journal*, 5, 1173–1181.

Rodrigues, C.T., EzEldeen, M., Jacobs, R., Lambrechts, P., Alcalde, M.P. & Hungaro Duarte, M.A. (2021) Cleaning efficacy and uncontrolled removal of dentin of two methods of irrigant activation in curved canals connected by an isthmus. *Australian Endodontic Journal*, 47, 631–638.

Schneider, S.W. (1971) A comparison of canal preparations in straight and curved root canals. *Oral Surgery, Oral Medicine, Oral Pathology, Oral Radiology, and Endodontology*, 32, 271–275.

Song, W., Hong, M., Lukyanchuk, B. & Chong, T. (2004) Laserinduced cavitation bubbles for cleaning of solid surfaces. *Journal of Applied Physics*, 95, 2952–2956.

Su, Z., Li, Z., Shen, Y., Bai, Y., Zheng, Y., Pan, C. et al. (2020) Characteristics of the Irrigant flow in a simulated Lateral Canal under two typical laser-activated irrigation regimens. *Lasers in Surgery and Medicine*, 53, 587–594. https://doi.org/10.1002/lsm.23317

Swimberghe, R.C.D., Buyse, R., Meire, M.A. & De Moor, R.J.G. (2021) Efficacy of different irrigation technique in simulated curved root canals. *Lasers in Medical Science*, 36, 1317–1322.

Swimberghe, R.C.D., Crabbé, A., De Moor, R.J.G., Coenye, T. & Meire, M.A. (2021) Model system parameters influence the sodium hypochlorite susceptibility of endodontic biofilms. *International Endodontic Journal*, 54, 1557–1570.

Swimberghe, R.C.D., De Clercq, A., De Moor, R.J.G. & Meire, M.A. (2019) Efficacy of sonically, ultrasonically and laser-activated irrigation in removing a biofilm-mimicking hydrogel from an isthmus model. *International Endodontic Journal*, 52, 515–523.

Tahmasbi, M., Jalali, P., Nair, M.K., Barghan, S. & Nair, U.P. (2017) Prevalence of middle mesial canals and isthmi in the mesial root of mandibular molars: an in vivo cone-beam computed tomographic study. *Journal of Endodontics*, 43, 1080–1083.

Versiani, M.A., De-Deus, G., Vera, J., Souza, E., Steier, L., Pécora, J.D., et al. (2015) 3D mapping of the irrigated areas of the root canal space using micro-computed tomography. *Clinical Oral Investigations*, 19, 859–866.

Villas-Boas, M.H., Bernardineli, N., Cavenago, B.C., Marciano, M., Del Carpio-Perochena, A., de Moraes, I.G. et al. (2011) Micro-computed tomography study of the internal anatomy of mesial root canals of mandibular molars. *Journal of Endodontics*, 37, 1682–1686.

Von Arx, T. (2005) Frequency and type of canal isthmuses in first molars detected by endoscopic inspection during periradicular surgery. *International Endodontic Journal*, 38, 160–168.

Weller, R.N., Niemczyk, S.P. & Kim, S. (1995) Incidence and position of the canal isthmus. Part 1. Mesiobuccal root of the maxillary first molar. *Journal of Endodontics*, 21, 380–383.

Yin, X., Chang, J.W.W., Wang, Q., Zhang, C. & Wang, X. (2021) Three-dimensional morphologic classifications and analysis of canal isthmuses in permanent molars. *Surgical and Radiologic Anatomy*, 43, 1793–1799.

SUPPORTING INFORMATION

Additional supporting information can be found online in the Supporting Information section at the end of this article.

How to cite this article: Robberecht, L., Delattre, J. & Meire, M. (2023) Isthmus morphology influences debridement efficacy of activated irrigation: A laboratory study involving biofilm mimicking hydrogel removal and high-speed imaging. *International Endodontic Journal*, 56, 118–127. Available from: https://doi.org/10.1111/iej.13836